Electronic structure and the glass transition in pnictide and chalcogenide semiconductor alloys. II. The intrinsic electronic midgap states

Andriy Zhugayevych[1] and Vassiliy Lubchenko[1,2,a)]
[1]*Department of Chemistry, University of Houston, Houston, Texas 77204-5003, USA*
[2]*Department of Physics, University of Houston, Houston, Texas 77204-5005, USA*

(Received 4 June 2010; accepted 17 October 2010; published online 16 December 2010)

We propose a structural model that treats in a unified fashion both the atomic motions and electronic excitations in quenched melts of pnictide and chalcogenide semiconductors. In Part I [A. Zhugayevych and V. Lubchenko, J. Chem. Phys. **133**, 234503 (2010)], we argued these quenched melts represent aperiodic $pp\sigma$-networks that are highly stable and, at the same time, structurally degenerate. These networks are characterized by a continuous range of coordination. Here we present a systematic way to classify these types of coordination in terms of discrete coordination defects in a parent structure defined on a simple cubic lattice. We identify the lowest energy coordination defects with the intrinsic midgap electronic states in semiconductor glasses, which were argued earlier to cause many of the unique optoelectronic anomalies in these materials. In addition, these coordination defects are mobile and correspond to the transition state configurations during the activated transport above the glass transition. The presence of the coordination defects may account for the puzzling discrepancy between the kinetic and thermodynamic fragility in chalcogenides. Finally, the proposed model recovers as limiting cases several popular types of bonding patterns proposed earlier including: valence-alternation pairs, hypervalent configurations, and homopolar bonds in heteropolar compounds. © *2010 American Institute of Physics*. [doi:10.1063/1.3511708]

I. INTRODUCTION

In the preceding article,[1] we presented a chemical bonding theory for an important class of pnictogen- and chalcogen-containing quenched melts and glasses. These materials exhibit many unique electronic and optical anomalies[2] not found in crystals and also are of great interest in applications such as information storage and processing.[3,4] We argued these materials can be thought of as aperiodic $pp\sigma$-networks made of deformed-linear chains that intersect at atomic sites at nearly right angles. Extended portions of the chains exhibit a perfect alternation of covalent and weaker, secondary bonds, even though the lattice as a whole is aperiodic. This bond alternation results from a symmetry breaking of a parent, simple cubic structure with octahedral coordination; this structure is uniformly covalently bonded. It is the intimate relation of the amorphous lattice to its covalently bonded parent structure that allowed us to rationalize, for the first time to our knowledge, two seemingly contradicting features of a bulk glass, i.e., its relative stability and structural degeneracy.[1]

Yet the argued presence of the degeneracy of the $pp\sigma$-network does not, by itself, guarantee that the network can be realized as an equilibrated supercooled liquid or a quenched glass. For instance, elemental arsenic can be made into an amorphous film but does not vitrify readily. To be a liquid, the network should contain a large equilibrium concentration of structural motifs corresponding to the transition states for activated transport in quenched melts.

The goal of the present article is to identify the bonding patterns of the transition-state structural motifs at the molecular level and describe the rather peculiar midgap electronic states that are intrinsically associated with such motifs. It will turn out that these electronic states are responsible for many of the aforementioned electronic and optical anomalies of amorphous chalcogenide alloys.

Identification of structural motifs in vitreous materials based on local coordination is difficult because the usual concept of coordination, which is not fully unambiguous even in periodic lattices, becomes even less compelling in aperiodic systems. Alternatively, one can try to classify such local motifs in terms of deviation from a putative reference structure, while assigning a corresponding energy cost. Such deviations could be called "defected configurations." However, in the absence of long-range order, defining a reference structure in vitreous systems is, again, ambiguous. To make an informal analogy, is there a way to identify a typo in a table of random numbers? The answer, of course, depends on the presence and specific type of correlation between the random numbers. The random first order transition (RFOT) theory[5] dictates that glasses do form subject to strict statistical rules prescribed by the precise degree of structural degeneracy of the lattice, implying that correlation functions of sufficiently high order should reveal defects, if any. In fact, already four-point correlation functions in space capture the length scale of the dynamic heterogeneity in quenched melts.[6–8] Yet the only type of order in glasses that appears to be unambiguously accessible to linear spectroscopy is the very shortest-range order. The very first coordination layer is usually straightforward to identify by diffraction experiments, while the strong covalent bonding between nearest neighbors is identifiable via the independent knowledge of the covalent radii of the pertinent elements. Already the next-nearest neighbor bonds

a)Author to whom correspondence should be addressed. Electronic mail: vas@uh.edu.

appear to exhibit a continuous range of strength and mutual angular orientation.

We have argued[1] aperiodic $pp\sigma$-networks naturally account for this flexibility in bonding in semiconductor glasses, while retaining overall stability. In doing so, we proposed a structural model, by which aperiodic $pp\sigma$-networks can be thought of as distorted versions of much simpler parent structures defined on the simple cubic lattice. There is no ambiguity whatsoever with defining coordination on a simple cubic lattice, thus allowing one to classify unambiguously the parent structures.

We will observe that the most important and essentially the sole type of defect in $pp\sigma$-bonded glasses is singly overcoordinated or undercoordinated atoms. These defects turn out to host peculiar midgap electronic states with the reversed charge–spin relation, i.e., chemically they resemble free radicals. We will argue that these defects in fact correspond to the electronic states residing on the high-strain regions intrinsic to the activated transport in semiconductor glasses proposed earlier by us.[9] On the one hand, these electronic states lie very deep in the forbidden gap. On the other hand, they are surprisingly extended, calling into question the adequacy of ultralocal defect models. This large spatial extent reveals itself by redistribution of the malcoordination over a large number of bonds, in a solitonic fashion, and delocalization of the wave function of the associated electronic state. The extended coordination defects are mobile, consistent with the conclusions of our earlier semi-phenomenological analysis[9] that the peculiar electronic states are hosted by high-strain regions that emerge during activated transport in quenched semiconductor melts.

The article is organized as follows. Section II reviews the conclusions of the RFOT theory on the concentration and spatial characteristics of the transition state configurations for activated transport in supercooled liquids and frozen glasses, and a general mechanism for the emergence of associated electronic states.[9] In Sec. III, a systematic classification of coordination defects in parent structures is carried out. In Sec. IV, we demonstrate that malcoordination defects in parent structures become delocalized in the actual, relaxed structure and make a connection with our earlier, semi-phenomenological analysis of the solitonic states.[9] When making this connection, we perform several independent consistency checks that the degeneracy of aperiodic $pp\sigma$-networks is indeed compatible with the degeneracy of actual semiconductor alloys. Lastly we argue that the electronic states make a temperature-independent contribution to the activation barrier for liquid reconfigurations, which helps explain the apparent disagreement between the thermodynamic and kinetic fragilities in chalcogenides.

We have alluded to two vulnerabilities of *ad hoc* defect theories, i.e., the difficulty in defining a putative reference structure and the presumption of defects' being ultralocal at the onset. Conversely, such *ad hoc* theories do not explain self-consistently how the defects combine to form an actual, quite stable lattice. The present approach resolves this potential ambiguity. First, since the defects are defined on a specific lattice in the first place, the question of their coexistence in a 3D structure is automatically answered. Second, as discussed in Sec. V, we will see how several popular defect theories proposed much earlier on phenomenological grounds are naturally recovered as the ultralocal limit of the present picture.

II. BRIEF REVIEW OF THE RFOT THEORY AND PREVIOUS WORK

Below we outline the minimum set of notions from the RFOT theory of the glass transition and other previous work, as necessary for the subsequent developments. Detailed reviews of the RFOT theory can be found elsewhere.[5,10]

Mass transport in liquids slows down with lowering temperature or increasing density because of increasingly more frequent molecular collisions. At viscosities of 10 P and above, however, the transport is no longer dominated by collisions but, instead, is in a distinct dynamical regime. The equilibrium liquid density profile[11] is no longer uniform, but instead consists of sharp disparate peaks,[12] whereby each atom vibrates around a fixed location in space for an extended period of time. In other words, the liquid is essentially an assembly of long-living structures that persist for times exceeding the typical relaxation times of the vibrations by at least three orders of magnitude.[13] Under these circumstances, mass transport becomes activated: atoms move cooperatively via barrier-crossing events whereby the current long-lived, low free energy aperiodic configuration transitions locally to another long-lived, low free energy configuration. The multiplicity of alternative aperiodic configurations is quantified using the so-called configurational entropy. A region of size N particles has $e^{s_c N/k_B}$ distinct structural states, where s_c is the configurational entropy per rigid group of atoms, often called the "bead."[13] The RFOT theory predicts that the configurational entropy at the glass transition is $\simeq 0.8 k_B$ per bead.[14]

Individual atomic displacements during the transitions are small, i.e., about the vibrational displacement at the mechanical stability edge, which is often called the Lindemann length d_L.[15] Although the activated transport regime is usually associated with supercooled liquids,[16,17] many covalently bonded substances, such as SiO_2, exhibit activated transport already above the melting point.[13]

During an activated reconfiguration, two distinct low-energy structures must coexist locally, implying that a higher free-energy interface region must be present. Because the interface separates aperiodic arrangements, it has no obvious structural signature; nonlinear spectroscopy is generally required to detect the interface. The transitions proceed in a nucleation like fashion; they are driven by the multiplicity of the configurations, subject to the mismatch penalty at the interface $\gamma\sqrt{N}$:[18,19]

$$F(N) = \gamma\sqrt{N} - T s_c N, \tag{1}$$

see Fig. 1. Here, N gives the number of beads contained within the nucleus and the coefficient $\gamma = \frac{3}{2}\sqrt{3\pi} k_B T \ln(a^2/d_L^2 \pi e)$.[14,20] The lengths a and $d_L \simeq 0.1a$ denote the volumetric size of a bead and the Lindemann displacement,[21] respectively. The reconfiguration

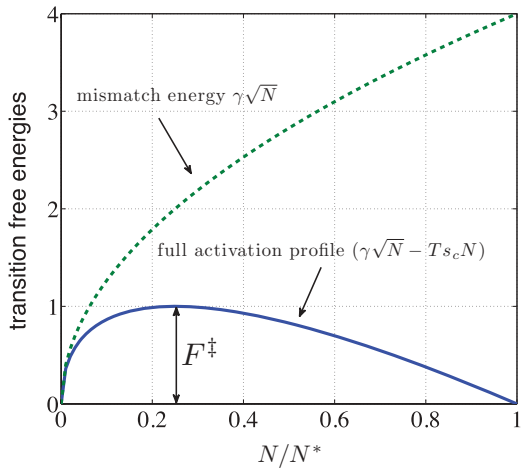

FIG. 1. Typical nucleation profile for structural reconfiguration in a supercooled liquid from Eq. (1) and its surface energy component $\gamma\sqrt{N}$, normalized by the typical barrier height, which reaches $(35-37)k_BT$ at $T = T_g$.

time corresponding to the the activation profile in Eq. (1)

$$\tau = \tau_0 e^{F^{\ddagger}/k_BT} = e^{\gamma^2/4Ts_c}, \tag{2}$$

grows in a super-Arrhenius fashion with lowering the temperature because of the rapid decrease of the configurational entropy[22,23]

$$s_c \simeq \Delta c_p T_g(1/T_K - 1/T), \tag{3}$$

where $\Delta c_p = T\partial s_c/\partial T|_{T_g}$ is the heat capacity jump at T_g per bead. The quantity T_K, often called the Kauzmann temperature or the "ideal glass" transition temperature, corresponds to the temperature at which the configurational entropy of an equilibrated liquid would presumably vanish. Hereby the log number of alternative configurations would scale sublinearly with the system size. While the temperature T_K appears in certain meanfield models,[24] the ideal-glass state, if any,[25] would be impossible to reach in actual liquids because of the diverging relaxation times, see Eq. (2).

The nucleus size

$$N^* \equiv (\gamma/Ts_c)^2, \tag{4}$$

where $F(N^*) = 0$, is special because it corresponds to a region size at which the system is guaranteed to find at least one typical liquid state. As a result, the size N^* corresponds to the smallest region that can reconfigure in equilibrium. Each transition requires work $\gamma\sqrt{N}$ to create and grow the interface, at the expense of relaxing the old interfaces. Thereby, the total number of interfaces remains constant on average. One thus concludes that the liquid harbors one interfacial region with an associated excess free energy $\gamma\sqrt{N^*}$ per region of size N^*, consistent with the quench being a higher free energy state than the corresponding crystal. In fact, the total mismatch penalty in a sample of size N is $\gamma\sqrt{N^*}(N/N^*) = Ts_cN$ and thus equals the enthalpy that would be released if the fluid crystallized at this temperature, save a small ambiguity stemming from possible differences in the vibrational entropies. The cooperativity size N^* grows with the decreasing configurational entropy[18] [see Eqs. (3) and (4)]: $N^*(T) \simeq N^*(T_g)[(T_g - T_K)/(T - T_K)]^2$. Still, it reaches only a modest value of 200 or so at the glass transition on 1 h time scale.[14,20] $N^*(T_g) = 200$ corresponds to a physical size $\xi \equiv a(N^*)^{1/3} \simeq 6.0\,a$, i.e., almost universally about two-three nanometers. This important prediction of the RFOT theory has been confirmed by a number of distinct experimental techniques [26–28] and recently, by direct imaging of the cooperative rearrangements on the surface of a metallic glass.[29] Now, the resulting concentration of the domain walls near the glass transition is, approximately,

$$n_{\mathrm{DW}}(T_g) \simeq 1/\xi(T_g)^3 \simeq 10^{20}\ \mathrm{cm}^{-3}. \tag{5}$$

In the rest of the article we will assume the material is just above its glass transition temperature T_g, so that it represents a very slow, but equilibrated liquid. Below T_g, the lattice remains essentially what it was at T_g, save some subtle changes stemming from the decreased vibrational amplitudes and aging.

The present authors have argued[9] that the interfaces may host special midgap electronic states, subject to a number of conditions. These conditions are satisfied in many amorphous chalcogenides and pnictides.[1] The number of the intrinsic midgap states is about two per interface, implying a concentration of about $2/\xi^3$, where ξ is the cooperativity length from Eq. (5). The argument in Ref. 9 is independent from the present considerations and is based on the RFOT theory of the glass transition.[5] These intrinsic states are centered on under- or over-coordinated atoms and are surprisingly extended for such deep midgap states. In addition, the states exhibit the reverse charge–spin relation. The existence of the intrinsic states allows one to rationalize a number of optoelectronic anomalies in chalcogenides in a unified fashion.[9] The interface-based electronic states in glasses are quasi-one dimensional and are relatively extended along that dimension.[9] This quasi-one dimensionality stems from the structural reconfigurations themselves being quasi-one dimensional: activated transitions between typical configurations occur by a nearly unique sequence of single-atom moves that are nearby in space. In the simplest possible Hamiltonian that couples electronic motions to the atomic moves, by which a transition between two metastable states takes place, only relative positions of the atoms are directly coupled to the electronic density matrix:[9]

$$\mathcal{H}_{\mathrm{el}} = \sum_{n,s}[(-1)^n\epsilon_n c^{\dagger}_{n,s}c_{n,s} - t_{n,n+1}(c^{\dagger}_{n,s}c_{n+1,s} + \mathrm{H.C.})], \tag{6}$$

where $c^{\dagger}_{n,s}$ $(c_{n,s})$ creates (removes) an electron on site n with spin s. The on-site energy, which reflects local electronegativity, is denoted with $(-1)^n\epsilon_n$. The electron transfer integral $t_{n,n+1}$ between sites n and $n+1$ depends on the intersite distance $d_{n,n+1}$. The sites are centered on beads, not atoms. The beads are numbered with index n, $1 \le n \le N^*$, in the order they would move during the reconfiguration.

III. CLASSIFICATION OF COORDINATION DEFECTS

The structural model proposed by us in Ref. 1 presents a systematic way to classify amorphous structures and the associated electronic-structure peculiarities in vitreous $pp\sigma$-networks. Without claiming complete generality, we will consider the following specific type of parent structures, which are largely based on Burdett and MacLarnan's model of (the crystalline) black phosphorous and rhombohedral arsenic.[30] In this model, each vertex on a simple cubic structure is connected to exactly three nearest neighbors, where only right angles are permitted between the links. Two specific periodic ways to place the links according to this prescription correspond to the crystals of black phosphorous and rhombohedral arsenic. We have seen that this model has a significantly broader applicability, if one allows for distinct atoms and also vacancies in the original cubic lattice. For instance, let us take the parent structure for black phosphorus [Fig. 5(b) of Ref. 1], place pnictogens and chalcogens in the rock salt fashion [as in Fig. 6(b) or 7 of Ref. 1], and then omit every third pnictogen in a particular fashion (as in Fig. 7 of Ref. 1). This procedure yields both the crystal structure and the stoichiometry of the archetypal pnictogen–chalcogenide compound Pn_2Ch_3 ("Pn" = pnictogen, "Ch" = chalcogen). In the crystal, each pnictogen and chalcogen are three- and two-coordinated, respectively, thus conforming to the octet rule.[31] The actual structure of a crystal or glass is thus viewed as a result of the following multistage procedure:[1] (1) start with the simple cubic structure with all vertices linked to all six nearest neighbors; (2) break the links and place vacancies to satisfy the stoichiometry and the octet rule. The resulting lowered-symmetry structure is called the "parent" structure. To generate the actual structure from the parent structure, (3) shift the atoms slightly toward the linked vertices; (4) turn on the interactions by associating an electronic transfer integral to each bond; and (5) geometrically optimize the structure, subject to the repulsion between the ionic cores and the variations in the electronegativity, if any.

In the above prescription, it is generally impossible to satisfy the stoichiometry and the octet rule at the same time except in the case of periodic crystals, as we will see explicitly in a moment. As a result, the resulting parent structure will generally exhibit a variety of defects in the form of under- and over-coordinated atoms, such as three-coordinated chalcogens. Similarly, incorporating elements of group 14, such as germanium, into the lattice of strictly three-coordinated vertices would introduce coordination defects. The just noted presence of four-coordinated vertices presents a convenient opportunity to point out that the hereby proposed structural model, though not unique, is special in the context of $pp\sigma$-bonded solids in distorted octahedral geometry. Suppose that, instead, we started from a model where each vertex is four coordinated. The corresponding parent structures, if periodic, could be unstable toward a tetrahedrally bonded solid with the β-tin or related structure.[32] As a result, the present discussion is likely limited to compounds where elements from group 14 are in the minority, except when these elements come in pairs with chalcogens, such as in GeSe or $Ge_2Sb_2Te_5$. Such pairs are isoelectronic with a pair of elemental pnictogens, and so both constituents of the pair are three coordinated. This is not unlike, for instance, how GaAs forms the diamond (zincblende) structure, in which each atom is four coordinated.

The three-coordinated parent structures on a simple cubic lattice, with right angles between the bonds, have another very special property:[30] in any lattice satisfying this constraint, whether periodic or not, each bond-containing line is a strictly alternating bond/gap pattern. Informally speaking, one may think of the lattice as made of linear chains, each of which consists of white and black segments of equal length in strict alternation; the junctions between adjacent segments correspond to the lattice vertices, while the white and black segments correspond to no-link and link, respectively. This observation allows one to easily estimate the number of all possible distinct parent structures. Since there are only two distinct ways to draw a perfect bond/gap alternating pattern, the total number of the parent structures in a sample of size $L_1 \times L_2 \times L_3$ with no vacancies is $2^{(L_1L_2+L_1L_3+L_2L_3)/a^2}$, where a is the lattice spacing. Note that in contrast to Ref. 30, we count as inequivalent two structures that can be obtained from each other by rotation, because they will both contribute to the phase space. We immediately observe that the total number of distinct parent structures is subthermodynamic in that it scales exponentially with the surface of the sample, not its volume. As a result, such defect-free structures cannot contribute significantly to the library of bulk aperiodic states. The only exception to this statement is the hypothetical Kauzmann, or ideal-glass state, in which the configurational entropy would strictly vanish.[33] One thus concludes that an equilibrium liquid must contain not only perfectly bond-alternating configurations, but also a finite number of defected configurations per unit length in each line, where a "defect" consists of two or more bonds (gaps) in a row.

Furthermore, parent structures of certain common stoichiometries, such as Pn_2Ch_3, must host a thermodynamic number of vacancies.[1] Adding vacancies to defectless aperiodic parent structures should generally lead to the creation of coordination defects. Indeed, to maintain the stoichiometry, the vacancies should be spaced on average by the same distance. On the other hand, one can construct a bond-breaking pattern with an arbitrarily large period, which can be made arbitrarily different from the average spacing between the vacancies.

As a consequence of the deviation from the strict alternation pattern along the individual linear chains, a thermodynamic number of atoms in a representative parent structure must be either under- or over-coordinated. Note that after geometric optimization, defects in the parent structure will be generally mitigated or even removed. For example, at least one of the covalent bonds around a four-coordinated pnictogen will generally elongate in the deformed structure, in the pnictogen's attempt to attain the favorable valency three. As a result, the overcoordination will be spread among a larger number of atoms. An example of defect annihilation is when an extra bond on an overcoordinated atom annihilates with a missing bond on a nearby undercoordinate vertex. For these reasons, a defect in the deformed lattice is not well defined. Here, we analyze several important defect configurations in

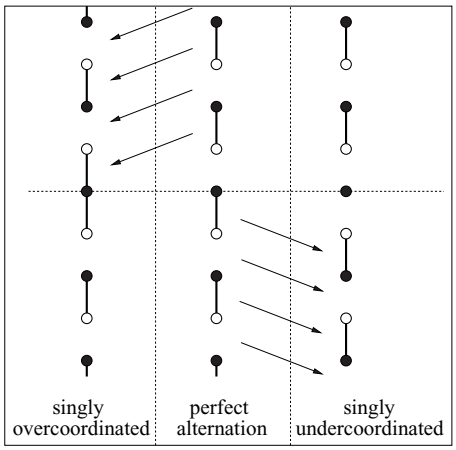

FIG. 2. Generation of singly malcoordinated atoms by a "cut-and-shift" procedure, see text. The filled and empty circles do not necessarily imply chemically distinct species, but are used to emphasize that it is the bond pattern that is shifted, not the atoms themselves.

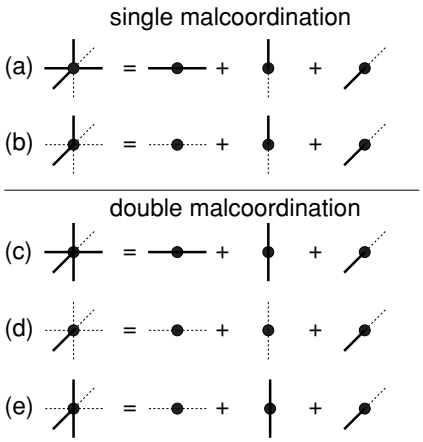

FIG. 3. Examples of malcoordination defects of different orders on a pnictogen site and their relation to single-malcoordination defects along individual directions. A similar diagram can be drawn for chalcogens, which are doubly coordinated in a defectless parent structure, the bond angle equal to 90°.

the parent structure, whereby the local coordination is entirely unambiguous. Before proceeding, we should note that the discussion is not limited to atoms of valence three and two. The above discussion applies even if a fraction of the vertices in the defectless parent structure should be four coordinated, as would be appropriate for elements of group 14. Estimating the total number of distinct parent structures is no longer straightforward; however, it is clear the number could be only lowered compared to the strict Burdett–McLarnan case.

Let us begin the discussion of defected parent structures with an ideal parent lattice with one singly overcoordinated vertex. This defect corresponds to two links in a row in one of the three chains crossing the vertex in question. Formally, one can obtain such a defect from a perfect Burdett–MacLarnan structure, for example, by choosing a vertex, removing the adjacent gap-segment from one of the chains and shifting the rest of the bond pattern on that side toward the vertex, see Fig. 2. Note that owing to $pp\pi$-interactions, such shift generally invokes an energy cost or gain in addition to the cost of overcoordinating the chosen vertex, which we will discuss later. One may obtain a singly undercoordinated vertex analogously, see Fig. 2. It is straightforward to see that more complicated, multiple-malcoordination configurations can always be presented as superpositions of the simple, single-malcoordination configurations described above, see Fig. 3. For instance, a doubly overcoordinated atom simply corresponds to overcoordination on two intersecting chains, at the vertex in question. Another common type of defect could be obtained by simply replacing a gap in an ideal parent structure by a link. This defect is equivalent to two singly overcoordinated atoms along the same line next two each other. Coordination defects of higher yet order can be constructed similarly. Note that bond angles other than 90° also amount to a coordination defect, even if the total number of bonds obeys the octet rule, see Fig. 3(e).

Single-malcoordination configurations can move along linear chains or make turns by bond switching, see Fig. 4, whereby the defect moves by two bond lengths at a time. Direct inspection shows, however, that an attempt to make a turn at a pnictogen in Fig. 4 (such as atom 4) will create a double defect, such as in Fig. 3(e), and is therefore likely to be energetically unfavorable. Generally, only turns on atoms of the same parity as the defect center are allowed. Note that the distance between the nearest singly over- and under-coordinated atoms, along a chain, should be always an even number of bonds, if the malcoordination is along the very same chain. These "opposite" defects can be brought together and mutually annihilated. Conversely, one observes that two opposite defects separated by an odd number of bonds cannot annihilate. A pair of such defects can be said to be topologically stable, see Fig. 5. In this Figure, we also illustrate that this pair of defects is mobile, subject to the "turning" rule above, of course. In addition, the specific defect-pair configuration in Fig. 5 is special because it allows for defect motion without the creation of Π-shaped bond motifs, in which three bonds constitute three sides of a rectangle. These motifs are somewhat energetically unfavorable, see the Appendix. Finally note that one of the nearest neighbors of the four-coordinated

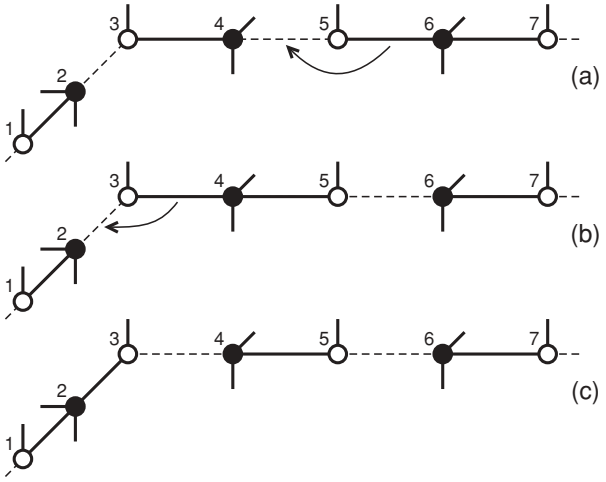

FIG. 4. Illustration of the motion of an overcoordination defect by bond-switching along a linear chain [from atom 6 in (a) to atom 4 in (b)] or making a turn [from atom 4 in (b) to atom 2 in (c)].

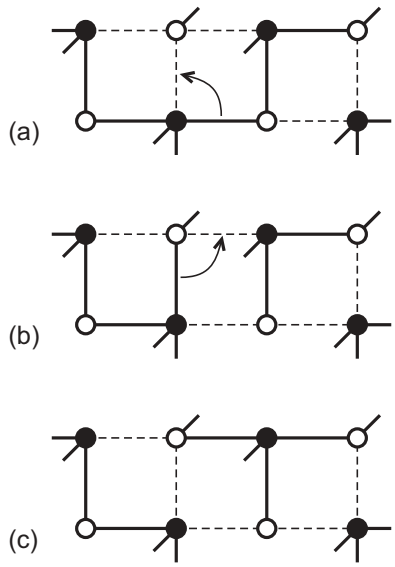

FIG. 5. A specific example of the motion of a topologically stable pair of an overcoordinated and undercoordinated defect, whereby the two defects move to the right while switching chains.

atom in Fig. 5(c) is not covalently bonded to any other atoms, implying the orientation of its bond with the central atom is relatively flexible. We will see below that owing to this extra flexibility and the said topological stability of the defect pair, the central atom is particularly unstable toward sp^3 hybridization when positively charged. Nevertheless, since each of the individual defects can be removed, such sp^3 hybridized units do not represent a distinct type of defect. Conversely, the formation of sp^3 hybridized atoms in $pp\sigma$-networks is reversible.

We thus conclude that singly malcoordinated atoms comprise the only distinct type of defect in the parent structure. The number of the motifs in the actual deformed structure that originate from the coordination defects in the parent structure is determined by the corresponding free energy cost. This cost consists of the energy cost proper of single-malcoordination defects, the energy of their interaction, and a favorable entropic contribution reflecting the multiplicity of distinct defect configurations. With regard to the interaction, it is easy to see that like defects should repel and defects of the opposite kind should attract. Indeed, the higher the over (under) coordination is, the larger the energy cost; conversely, mutual annihilation of a singly overcoordinated and undercoordinated defects is energetically favorable. One may thus conclude that for both energetic and entropic reasons, there are no bound states of single-malcoordination defects to speak of that could be classified as a distinct type of defect. The only such bound state is a topologically stable pair of a singly overcoordinated and undercoordinated vertex, as in Fig. 5.

We have pointed out earlier[1] that defectless parent structures can be formally represented as a subset of configurations of the 64-vertex model, which is the 3D generalization of the six-vertex model of ice and eight-vertex model of antiferroelectrics.[34] The presence of malcoordination can still be implemented in the 64-vertex model, by assigning an appropriate energy cost to such coordination. However, the presence of $pp\pi$-interaction implies nonadjacent bonds interact directly. One concludes that parent structures of pertinence to $pp\sigma$-networks are subject to a more general class of models, such as the Ising model with next nearest interactions.[34]

In concluding the discussion of defect classification, we emphasize that stoichiometry-based vacancies in parent structures should be regarded not as defects, but as an intrinsic part of the parent structure. As in the example of the parent Pn_2Ch_3 structure,[1] such stoichiometry-based vacancies contribute to driving the distortion of the original simple cubic lattice and are minimized in the deformed structure, subject to competing interactions. Formally, this means the energy cost of local negative density fluctuations in the deformed structure that stem from the vacancies in the parent structure is a perturbation to the $pp\sigma$ bonding, similarly to the sp-mixing. Elementary estimates of the energy cost of a vacancy in a glass[35] show the cost is prohibitively high, dictating that an equilibrium melt above the glass transition will contain negligibly few voids of atomic size or larger. Similarly, homopolar bonds are not regarded as defects from the viewpoint of the present structural model. In fact, we have argued[1] a thermodynamic quantity of homopolar bonds in parent structures are required for the presence of transport in supercooled melts. These notions are consistent with the relatively low electronegativity variations in $pp\sigma$-bonded materials[1] and hence a weak applicability of Pauling's rules.[31] To avoid possible confusion, we reiterate that the present argument strictly applies only to equilibrium melts or to glass obtained by quenching such melts. Amorphous films made by deposition generally do not correspond to an equilibrated structure at any temperature and, presumably, could host a greater variety of structural motifs.

IV. THE INTRINSIC MIDGAP ELECTRONIC STATES

To characterize the motifs arising in the deformed structure as a result of one singly undercoordinated atom in a parent structure, we consider first an isolated chain of $pp\sigma$-bonded arsenic atoms passivated by hydrogens: $(AsH_2)_n$. For concreteness, the chain is oriented along the z axis. An infinite undistorted chain is Peierls-unstable.[1] The two ground state configurations of an infinite $(AsH_2)_n$ chain consist each of a perfect alternation pattern of covalent and secondary bonds. A good approximation for these ground states can be obtained using a finite linear chain containing an even number of monomers, see the preceding article.[1]

Even if the chain is embedded in a lattice, each of these two ground states can still be regarded as the result of a Peierls transition, so long as the deviation from the strict octahedral coordination is weak. It is shown in Ref. 1 that the $pp\sigma$-chain portion of the full one-particle wave-function is an eigenfunction of the effective Hamiltonian:

$$\tilde{\mathcal{H}} = \mathcal{H}_{pp\sigma} + \mathcal{V}^{\dagger}(E - \mathcal{H}_{\text{env}})^{-1}\mathcal{V} \tag{7}$$

with the same eigenvalue E, where $\mathcal{H}_{pp\sigma}$ contains exclusively the p orbitals in question, $\mathcal{H}_{\text{env}}$ the rest of the orbitals, and $\mathcal{V}$ the transfer integrals between the two sets of orbitals. Using Eq. (7), the effect of the environment can be presented as an (energy dependent) renormalization of the on-site

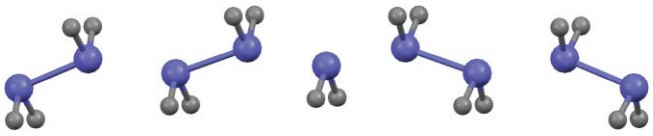

FIG. 6. Central part of neutral $(AsH_2)_{21}$ chain, whose ground state contain a coordination defect and the associated midgap level. The calculations are performed on semiempirical level by MOPAC (Ref. 36) with PM6 parametrization and the RHF/ROHF (Restricted Hartree–Fock and Restricted Open-shell Hartree–Fock) method, see Ref. 1 for full computational detail and supplementary material (Ref. 47) for comparison between the results of optimization for several chain lengths.

energies and transfer integrals of the $pp\sigma$-network proper, see Appendix C of Ref. 1. The most significant contributor to this perturbation is the competing sp interactions. The perturbation resulting from these competing interactions turns out to be sufficiently weak, as could be inferred from (a) its magnitude being close to the corresponding estimate using a perturbation series in the lowest non trivial order; and (b) the bond morphology in the chain conforming to what is expected from a $pp\sigma$-network.[1]

Now, in contrast to an even-numbered chain, the ground state of a $(4n+1)$-membered open chain can be thought of as having one singly undercoordinated atom, see Fig. 6, while the ground state of a $(4n+3)$-membered open chain contains one singly overcoordinated atom. Either of these "defected" chains is a neutral radical with an unpaired spin. The spectrum of the defected chain, shown with crosses in Fig. 7, exhibits a singly populated state exactly in the middle of the forbidden gap. The electronic wave function of this midgap state, shown in Fig. 8, is centered on the undercoordinated atom and exhibits a significant degree of delocalization. Likewise, the deviation from the perfect bond alternation, although the strongest in the middle of the chain, is delocalized over several atoms. The partitioning of the electronic density between the p_z orbitals proper (73%), the arsenics' s-orbitals (21%), and the rest of the orbitals (6%) indicate that the interactions that compete with the $pp\sigma$-bonding proper are significant but, nevertheless, may be regarded as a perturbation to the latter bonding, similarly to the perfectly dimerized chain.[1] Note that the position of the nodes of the wave-function is easy to understand using elementary Hückel considerations: consider an odd-numbered

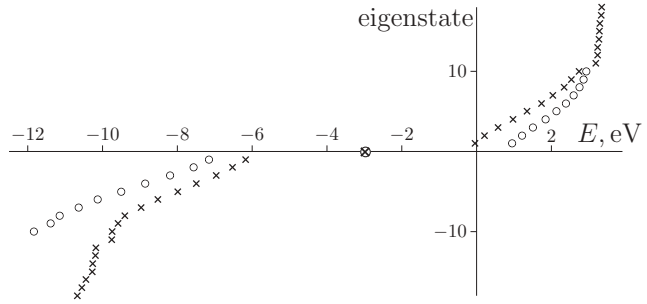

FIG. 7. Electronic energy levels of the defected chain $(AsH_2)_{21}$ chain from Fig. 6: full MO calculation (crosses) vs one-orbital model with renormalized $pp\sigma$ integrals (circles). States below the gap are filled; the midgap state is half-filled.

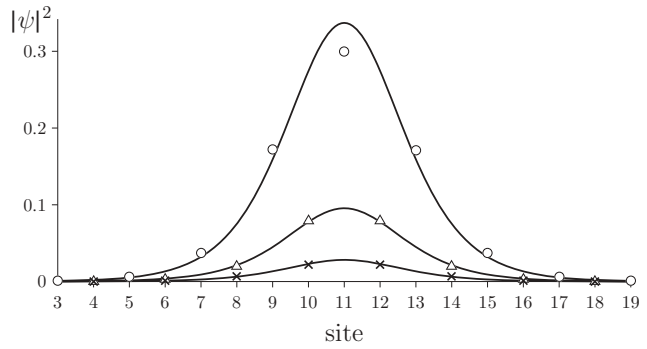

FIG. 8. The wave function squared of the midgap state of the $(AsH_2)_{21}$ chain: the circles correspond to the arsenics' p_z atomic orbitals (AO) (total contribution 73%), triangles As s-AO's (21%), crosses—the rest of AO's (6%). All contributions are nearly zero on every other atom; these very small values are omitted for clarity. The solid line corresponds to Eq. (10).

chain of identical atoms, each hosting an odd number of orbitals. A moment thought shows that the resulting set of orbitals (in one electron approximation) has a half-filled non bonding orbital, whereby the wave-function has nodes on every second atom.

The delocalization of the malcoordination is manifest in the broad sigmoidal profile of the $pp\sigma$ transfer integral as a function of the coordinate, see Fig. 9. Because the malcoordination is distributed among a large number of bonds in the deformed structure, the resulting structural signature of such a defect is far from obvious. In fact, the magnitude of the transfer integrals for the bonds adjacent to the overcoordinated atom in a $(4n+3)$ chain is very similar to that for the undercoordinated atom in a $(4n+1)$ chain. This magnitude is approximately the average of the magnitude of the transfer integral for the covalent and secondary bond in a perfectly dimerized chain, see Fig. 9. The same comment applies to the corresponding bond lengths in the first place, see Fig. 11, in view of the direct relationship between d and t. As a result, the malcoordination is essentially fully "absorbed" by the chain. For instance, the distances between atoms 1 and 19 in 19- and 21-member chains are 48.71 and 48.70 Å, respectively. These notions emphasize yet another time the ambiguity of defining coordination or coordination defects in actual,

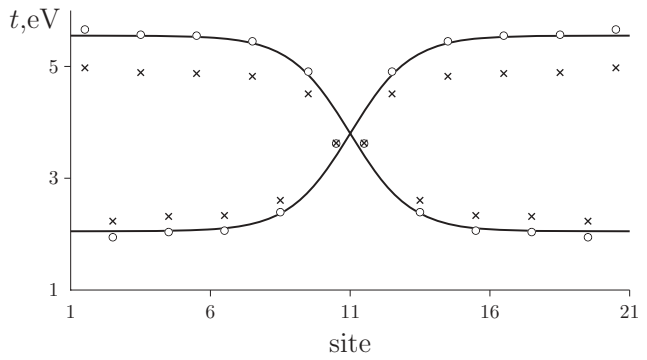

FIG. 9. Spatial dependence of the $pp\sigma$ transfer integral in the $(AsH_2)_{21}$ chain. The actual transfer integrals from $\mathcal{H}_{pp\sigma}$ in Eq. (7) are shown with crosses. The renormalized integrals from $\widetilde{\mathcal{H}}$ in Eq. (7) are shown with circles. The solid line corresponds to Eq. (8).

deformed structures. Despite being relatively extended, the undercoordination defect could be thought of as separating two alternative states with perfect dimerization. This defect exhibits the reverse charge–spin relation, because it is neutral when its spin is equal 1/2. Adding or removing an electron would yield a singly charged defect with spin 0. These characteristics of the midgap state in the $(AsH_2)_n$ chain are entirely analogous to those of the midgap state in *trans*-polyacetylene, which is a classic example of a Peierls insulator. Until further notice, we will consider only neutral chains. Unlike the perfectly dimerized chain, a geometry optimized defected chain is somewhat curved on average; this effect is small, however.

The surprisingly large spatial extent of the midgap state in the arsenic chain results from an interplay of several factors, similarly to how the spatial characteristics of the solitonic state in polyacetylene depend on the lattice stiffness, electronic interactions, etc. Nevertheless, it turns out that in both systems the extent of delocalization is determined essentially by only two parameters, namely the renormalized transfer integrals of the covalent and secondary bond in the perfectly dimerized chain, denoted with t and t', respectively. (In the case of polyacetylene, the transfer integrals are $pp\pi$, of course.) This simplification takes place because, similarly to the case of a perfectly dimerized chain, the effects of the competing intrachain and external interactions on the midgap state largely reduce to the renormalization of the $pp\sigma$ interaction proper. To demonstrate this notion, we take the geometrically optimized chain, extract only the $pp\sigma$ integrals, and renormalize them according to Eq. (7) while setting E equal exactly to the center of the forbidden gap. The spectrum of the resulting Hamiltonian is shown with circles in Fig. 7. Setting E at the center of the gap should result in an error the greater, the further the state in question from the gap center. Yet one infers from Fig. 7 that the error in the spectrum is relatively small, consistent with the smallness of the perturbation.

The spatial dependence of the renormalized $pp\sigma$ integrals is shown in Fig. 9 with circles. In the continuum limit[37] of the Su–Schreiffer–Heeger (SSH) model for midgap states in *trans*-polyacetylene,[37] the transfer integral depends on the coordinate according to the expression:[9]

$$t_n = \frac{t+t'}{2} + \frac{t-t'}{2}(-1)^n \tanh\left(\frac{n-n_0}{\xi_s/d}\right), \tag{8}$$

where the soliton is centered on bond n_0 and its half-width ξ_s is given by[9]

$$\xi_s = \frac{t+t'}{t-t'}d, \tag{9}$$

where d is the length of the bond in the parent structure. Using the renormalized values of the parameters t and t' from Ref. 1, we obtain the solitonic profile shown by the solid line in Fig. 9. Note the difference between the two sets of transfer integrals is small. Finally, the electronic wavefunction in the same continuum limit is given by the function:

$$\psi_n^2 = (1/2)(d/\xi_s)\cosh^{-2}[(n-n_0)d/\xi_s], \tag{10}$$

as shown with the solid lines in Fig. 8. Again, the agreement with the result of an electronic structure calculation using renormalized transfer integrals is good. The agreement is not expected to be perfect, however, because of the approximations inherent in the continuum limit[37] of the SSH model.

We thus observe that to describe both the ground state and defected configurations of linear chains from a $pp\sigma$ network, we can apply a Hamiltonian that contains explicitly only the $pp\sigma$ interactions whose parameters are renormalized by other interactions. This resulting tight-binding Hamiltonian, which corresponds with the renormalized Hamiltonian (7), reads as:

$$\mathcal{H}_{\rm el} = \sum_{n,s}[(-1)^n \epsilon_n c_{n,s}^\dagger c_{n,s} - t_{n,n+1}(c_{n,s}^\dagger c_{n+1,s} + \text{H.C.})], \tag{11}$$

where $c_{n,s}^\dagger$ ($c_{n,s}$) creates (annihilates) an electron with spin s in the p_z-orbital on atom n. The on-site energy, which reflects the local electronegativity, is denoted with $(-1)^n\epsilon_n$. The renormalized electron transfer integral $t_{n,n+1}$ between sites n and $n+1$ depends on the bond length $d_{n,n+1}$. The latter is determined by the restoring force of the lattice, in addition to the Peierls symmetry breaking force stemming from the electronic degree of freedom in Eq. (11). The restoring force of the lattice includes both the intra chain and extra chain perturbations to the $pp\sigma$ interaction. We have seen in Ref. 1 that a portion of the intra chain perturbation, namely the sp-mixing also contributes to the symmetry-breaking that results in bond-dimerization of the chain. Yet according to Eqs. (9) and (10), the participating competing interactions determine the spatial characteristics of the coordination defect largely through the values of only two parameters: t and t', in addition to the lattice spacing d.

We are now ready to argue that the defect states centered on singly malcoordinated atoms in $pp\sigma$-chains, as in Figs. 7–9 should be identified with the intrinsic states proposed in Ref. 9. On the one hand, $pp\sigma$-bonded glasses meet the sufficient conditions for the presence of the intrinsic states, as argued in the preceding article.[1] On the other hand, we have seen here a singly malcoordinated atom is the only type of defect present in $pp\sigma$-bonded glasses, while all of its characteristics are identical to those established independently for the intrinsic states, including the reverse charge–spin relation and the relative delocalization. In addition, both types of states emerge at the coexistence region of two distinct lowered-symmetry states, which originated from a higher symmetry state. In the rest of this section, we discuss the microscopic insights arising from both the common aspects and complementarity of the semi-phenomenological approach from Ref. 9 (case 1) and the present, molecular model for the midgap states in $pp\sigma$-bonded glasses (case 2).

Let us begin with the electronic Hamiltonian governing the formation of the midgap states. In both cases, the electronic Hamiltonians are quasi one dimensional, whereby the sites are situated along a deformed line in space. Although the Hamiltonians are identical notation-wise, they are distinct microscopically: In case 1, Eq. (6), the sites refer to rigid molecular units, often called "beads." By construction, the beads are not significantly disturbed by liquid motions and, conversely, interact only weakly with each other, comparably to the van der Waals coupling. Beads usually contain several atoms each; they are essentially chemically equivalent

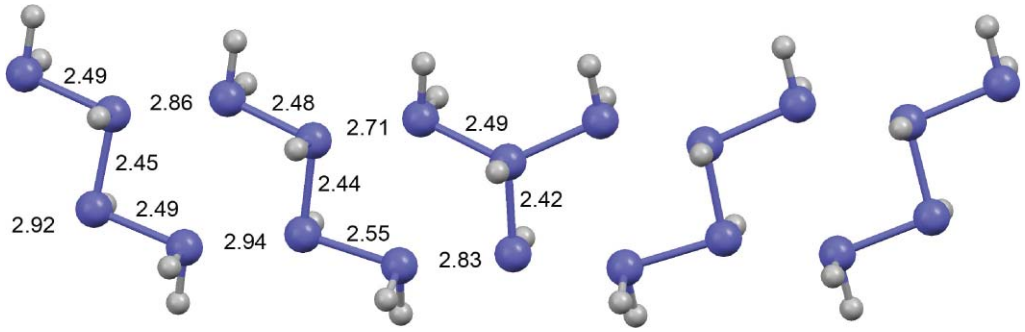

FIG. 10. Central portion of a geometrically optimized double chain of hydrogen-passivated arsenics. The top and bottom chains, containing 19 and 17 arsenics, host an overcoordinated and undercoordinated arsenic, respectively, cf., Fig. 6. The numbers denote the bond lengths in Angstroms.

and fill out the space uniformly. The volumetric size of the bead is denoted with a.[13] In contrast, in case 2, Eq. (11), the sites are actual atomic orbitals which are generally not chemically equivalent. To check whether the two Hamiltonians are consistent, we recall the RFOT theory's prediction that the smallest cooperativity size ξ is just above $2a$,[13] implying a supercooled melt can host at most one malcoordinated atom per ~4 beads at the onset of activated transport at a temperature T_{cr}. The volumetric size a of the bead can be estimated based on the RFOT's prediction that the configurational entropy at the glass transition on 1 h time scale is universally 0.8 per bead.[14] For As_2Se_3, this estimate yields about a half of the As_2Se_3 unit per bead, i.e., roughly one bead per arsenic atom, and $a \simeq 4.0$ Å.[9] An inspection of the parent structure of As_2Se_3 in Fig. 8 of Ref. 1 demonstrates that it is possible to accommodate one malcoordination defect per four arsenics so that the defects are separated by at least two atoms. Since the defects are not immediately adjacent in space, the geometric optimization of the parent structure will not necessarily lead to their mutual annihilation.

Next, we address the width of the interface and the related restriction on the spatial variation of the electronic transfer integral. In Ref. 9, we used the simplest spatial profile of bead displacement during a cooperative rearrangement to suggest that the soliton half-width ξ_s is bounded from below by $\xi/2$, which is about $3a$ at T_g. Inspection of Fig. 9 indicates that the soliton, though still extended, is somewhat more narrow, i.e., $\xi_s \simeq 2a$. (Recall also that $d < a$.) Using the condition[9]

$$\xi_s < \frac{t+t'}{t-t'}a, \tag{12}$$

we then should revise the lower limit on the variation of the transfer matrix element to:

$$t'/t \gtrsim 0.3. \tag{13}$$

We have seen earlier[1] that the $pp\sigma$-bonded materials in question do indeed meet this revised condition very well. Finally we note that the prediction of Ref. 9 that the extent of the wave function somewhat exceeds $2\xi_s$ is indeed borne out by the result in Fig. 8.

The RFOT theory makes specific predictions as to the free energy cost of a structural reconfiguration. For instance, the total mismatch penalty near the glass transition, according to the discussion of Fig. 1, is four times the typical barrier for the reconfiguration. At the glass transition, this corresponds to about $140k_BT_g$, or generically about 3–4 eV. For the present microscopic picture to be valid, this energy should exceed the energy cost of the structural defect, which includes the energy of the associated lattice deformation and the electronic energy proper. We have established earlier[9] that the electronic energy associated with the intrinsic state can be estimated via the optical gap E_{gap} and the effective attraction U_{eff} between like particles occupying the state: $\sim(E_{gap} - |U_{eff}|) \simeq 0.7E_{gap}$. This figure is about one quarter of the full interface energy predicted by the RFOT theory. Alternatively, according to the solution of the continuum limit of the SSH model, the cost of the intrinsic state on an isolated defect can be expressed through its width ξ_s:

$$\frac{4}{\pi}\frac{t}{1+\xi_s/a}, \tag{14}$$

yielding a similar figure to the above estimate. One observes that, indeed, the present microscopic picture is internally consistent. There yet is another potential electronic contribution to the defect energy. We have already mentioned that the creation or motion of a defect may by accompanied by a creation of Π like patterns of bonds in the parent structure; the latter are analyzed in the Appendix.

A chain hosting a singly under- and over-coordinated defect can always lower its energy via mutual annihilation of the defects, consistent with conclusions of the continuum approach of Ref. 9 Two such defects on different chains, however, may be topologically stable against such annihilation, as in Fig. 5(c). Such a configuration presents a felicitous opportunity to examine the interaction of the defects in the deformed structure, for instance, by geometrically optimizing a double $(4n+1)-(4n+3)$ chain of hydrogen-passivated arsenics, see Fig. 10. One observes that in the ground state of a resulting defect pair, the under (over) coordinated atom is negatively (positively) charged, so as to obey the octet rule, see also Sec. V. The resulting dipole moment of the chain is 3.3 D; see the shapes of the HOMO/LUMO orbitals and electrostatic map of the chain in the Supplementary Material.[47] The As–As angles at the overcordinated arsenic are 110°, 110°, and 128°. Note in perfect tetrahedral coordination, these angles would be 109.5°. In addition, the defects become more localized when in close proximity, as shown in Fig. 11, because of the partial cancellation of the

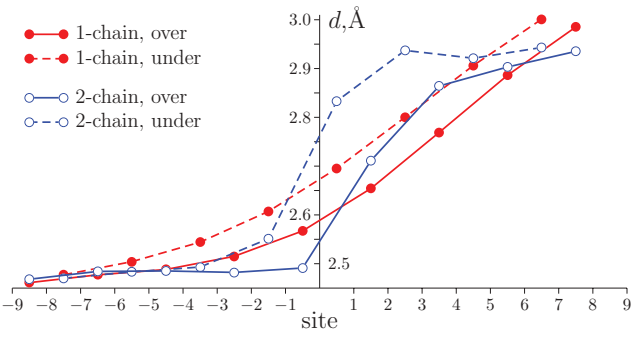

FIG. 11. Site dependence of the As–As bond length in single and double chains of hydrogen-passivated arsenics, as labeled by "1-chain" and "2-chain," respectively. The "1-chain, under" corresponds to a $(AsH_2)_{17}$ chain similar to the $(AsH_2)_{21}$ chain from Fig. 6 and "1-chain, over" corresponds to a $(AsH_2)_{19}$ chain. The double-chain entries pertain to the individual chains in Fig. 10, "over" and "under" correspond to the top and bottom chain, respectively.

malcoordination. Alternatively, one may say the energy cost of this localization partially offsets the stabilization resulting from the binding of the defects.

The extended nature of the coordination defects is consistent with their mobility: in the continuum limit, the pinning of a soliton is in fact strictly zero. Consistent with the latter notions, the energy gradients during geometrical optimization of the $(AsH_2)_n$ chain above have very small numerical values. Notwithstanding this complication, an estimate for the barrier for soliton hopping event (by two bond lengths) can be made within the SSH model: using the effective transfer integrals from Eqs. (8) and (9) we estimate the energy of the transition state configuration (corresponding to a move by one bond length) at approximately 0.1 meV, which is about $10^{-5}E_{\text{gap}}$. $pp\pi$ interactions may also contribute to pinning, see the Appendix for quantitative estimates. While the above notions may apply relatively directly to neutral defects even in actual 3D lattices, the situation appears to be more complicated for charged solitons (which in fact greatly outnumber the neutral ones[9]) because of lattice polarization. This is work in progress. Finally, note the high mobility of the soliton seems particularly important in the context of cryogenic anomalies of glasses, which have been argued to arise from the low-barrier subset of the structural reconfigurations.[10,20]

As an additional dividend of the present discussion, let us see that the presence of an electronic—and hence T-independent—contribution to the RFOT's mismatch penalty between distinct low free energy aperiodic configurations allows one to partially explain the deviation of chalcogenides from the RFOT-predicted correlation between the thermodynamics and kinetics of the glass transition. Indeed, because of this T-independent contribution we expect corrections to the detailed temperature dependence of the reconfiguration barrier $F^{\ddagger}$ from Eq. (2) and the value of the so-called fragility coefficient $m = (1/T)\partial \log(\tau)/\partial(1/T)|_{T=T_g}$.[13,38] The RFOT theory predicts that this coefficient should be equal to what one may call a "thermodynamically" determined fragility $m_{\text{thermo}} = 34.7 \times \Delta c_p(T_g)$ where $\Delta c_p(T_g)$ is the heat capacity jump at the glass transition per bead.[13,47] Using the measured $\Delta c_p(T_g)$ per mole, and the bead size determination from the fusion enthalpy produces excellent agreement for dozens of substances;[38] however, among the outliers are the chalcogenides. For instance, for As_2Se_3, the measured $m \simeq 40$, while the theoretically computed $m_{\text{thermo}} \simeq 7.5$. Determination of the bead size is ambiguous in As_2Se_3, because the corresponding crystal is highly anisotropic. In fact, in the fusion-entropy based estimate, the bead comes out to be about a single atom, in conflict with the aforementioned requirement of chemical homogeneity and with Ref. 39, where a bead was argued to contain at least two atoms. Using the RFOT's prediction that $s_c(T_g) \simeq 0.8k_B$ per bead, gives a better value $m_{\text{thermo}} \simeq 17$,[9] still not enough to account for the disagreement. Simple algebra shows that in the presence of a T-independent contribution to the surface tension, the estimate of the thermodynamic fragility from Ref. 13 should be increased by a factor of $[1 + 2(\delta\Sigma)(T_g - T_K)/T_K]$, where $\delta\Sigma$ is the relative contribution of the electronic states to the total surface energy at T_g. Assuming the mentioned $\delta\Sigma \simeq 0.25$ and using parameters for As_2Se_3 from Ref. 9, we get an increase by a factor of 1.45, which is a considerable correction in the right direction. Besides the experimental uncertainty in determination of T_K, we note also that more than one pair of solitonic states might accompany the transition. This would significantly increase the corresponding contribution to the surface tension and the fragility.

We note that since $(T_g - T_K)/T_K \propto 1/\Delta c_p$, this T-independent correction to the surface tension would be less significant for fragile substances. $[(T_g - T_K)/T_K \lesssim 1$ for known substances]. This reflects the old notion that the temperature dependence of s_c is the leading contribution to the viscous slowdown in a supercooled melt, except in strong liquids whose slowdown is nearly Arrhenius-like. Incidentally, the strongest liquids from the survey by Stevenson and Wolynes,[38] namely GeO_2, and BeF_2, and $ZnCl_2$, do conform to the relation $m_{\text{thermo}} = 34.7 \times \Delta c_p(T_g)$. This is consistent with the present results, since we do not expect solitonic states in these wide-gap materials.

V. THE CHARGE ON THE COORDINATION DEFECTS AND THE RELATION TO EARLIER DEFECT THEORIES

We have argued previously[9] that the intrinsic midgap states should be typically charged: a half-filled defect is essentially a neutral molecule embedded in a dielectric medium and should be generally stabilized by adding a charge, because of ensuing polarization. To analyze distinct charge states of the coordination defects in the present approach, we will use the same methodology as in Sec. III and Sec. IV above: we will consider distinct charge states on the defects in the parent structure, with the usual understanding that the corresponding motif in the actual, deformed structure will be significantly delocalized. It is during the analysis of charged defects in the parent structure that we will be able to make a connection between the present approach and the much earlier specific proposals on the defect states in chalcogenides.[40,41]

The large spatial extent of the malcoordination-based states is a result of the lattice's attempt to mitigate the energy cost of what would have been a local defect in the parent structure. The converse is also true. According to Eq. (14), the

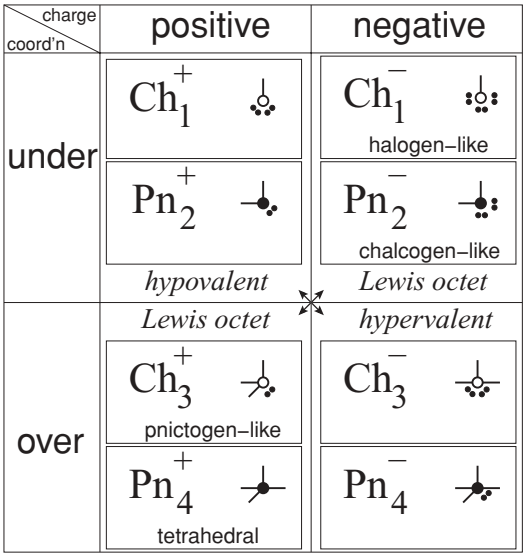

FIG. 12. A compilation of the possible charged states of singly malcoordinated atoms. Here, "Ch" = chalcogen, "Pn" = pnictogen. Neutral states, not shown, imply dangling bonds and would be energetically costly.

energy cost of localizing malcoordination would well exceed the energy density typical of an equilibrium melt. Thus in the analogies below between the present and earlier approaches, one should keep in mind that on the one hand, the earlier proposals ascribing midgap states to specific local defects can be thought of as an ultralocal limit of the present theory. On the other hand, we see that this ultralocal limit is somewhat artificial in that it greatly overestimates the energy cost of the defects.

Because there is only one basic type of the defect, namely a singly under- or over-coordinated atom, and three distinct charges: $-1, 0, 1$, the possible combinations of these variables are only few, see Fig. 12. Already an elementary analysis yields that charged states are expected to be stabilized, consistent with independent arguments from Ref. 9. Indeed, four of the resulting configurations, namely those listed in the "Lewis octet" sectors, satisfy the octet rules and thus are expected to be particularly stable. Specifically, a positively charged overcoordinated chalcogen is chemically equivalent to a pnictogen and a negatively charged undercoordinated pnictogen is equivalent to a chalcogen. These two configurations are expected to stabilize the distorted octahedral arrangement of the ambient lattice. On the other hand, the Pn_4^+ configuration is unstable toward tetrahedral order, cf., Figs. 5(c) and 10, and as such, would tend to frustrate the $pp\sigma$-network. The situation with the entries in the "hypervalent" and "hypovalent" sectors appears less certain. First off, we have used the label "hypervalent" in the right bottom sector in reference to the formal electron count around the atom exceeding eight and the low magnitude of electronegativity variation in the compounds in question. The T-shaped bond geometry in the Ch_3^- case was chosen by analogy with small molecules with the same electron count, such as ClF_3. If the T-shaped bond geometry is indeed favored for this type of defect, there will be an additional penalty for a negatively charged defect to make a turn at a chalcogen. Now, the left upper section represents a hypovalent configuration. In the worst case, these hypovalent configurations would favor a triangular bipyramidal arrangement, in which there is linear alignment for at least two bonds. We have not listed neutral defects in the table. These would amount to having dangling bonds and thus are deemed energetically costly. Finally note that pairs of oppositely charged defects with complementary coordinations will either annihilate or be particularly stable, if their annihilation is topologically forbidden. This attraction is indicated by the double-ended arrows in Fig. 12. A specific realization of an attractive, topologically stable pair of defects in a deformed structure is shown in Fig. 10. This configuration formally corresponds to a bound Pn_2^-–Pn_4^+ pair.

Several specific configurations from Fig. 12, including Ch_3^+, Ch_3^-, Ch_1^+, and Pn_4^+ have been proposed as relevant defect species earlier, based on the putative presence of dangling bonds[39,40] vector-type charge–density waves,[44] and molecular dynamics studies using energies determined by tight-binding methods.[45] Specifically in the venerable approach of Kastner *et al.*,[39] pairs of defects, called valence-alternation pairs (VAP), could spontaneously arise in glass because of a presumed instability of a pair of dangling bonds toward creation of two charged defects: $2Ch_3^0 \rightarrow Ch_3^+ + Ch_1^-$ or $2Pn_4^0 \rightarrow Pn_4^+ + Ch_1^-$. Despite common features with the VAP theory, the present picture is distinct in several key aspects, in addition to the aforementioned ones. We have seen in Sec. III the coordination defects are a necessary prerequisite for molecular transport and are themselves mobile. In other words (the delocalized versions of) the specific configurations from Fig. 12 are simply transient configurations arising during motions of the structural interfaces in a quenched melt or frozen glass.

VI. CONCLUDING REMARKS

We have proposed a structural model, by which the structure and electronic anomalies of an important class of vitreous alloys emerge in a self-consistent fashion. The model allows one to reconcile two seemingly conflicting characteristics of quenched melts and frozen glasses. On the one hand, these materials exhibit remarkable thermodynamic and mechanical stability, only slightly inferior to the corresponding crystals. On the other hand, these materials are also multiply degenerate thus allowing for molecular transport. The stability of the lattice stems from its close relationship with a highly symmetric, fully bonded structure.[1] The lattice's aperiodicity and the necessary presence of a thermodynamic number of transition states for structural reconfigurations dictate that the lattice exhibit a thermodynamic number of special structural motifs, roughly one per several hundred atoms at T_g. These motifs host midgap electronic states that are similar to solitonic states in *trans*-polyacetylene.[46] The motifs correspond to coordination defects in the parent structure, which can be defined entirely unambigously. In contrast, in the actual materials, coordination is poorly defined because the interatomic distances and bond angles are continuously distributed. The presence and the characteristics of these defects have been established using an exhaustive, systematic protocol, implying the classification of the defects is complete.

The actual molecular mechanism of both the stability of semiconductor glasses and the mobility of the defected configurations relies on the very special property of chalcogen- and pnictogen-containing semiconductors, namely their fully developed $pp\sigma$-bond network. Hereby, most atoms exhibit a distorted octahedral coordination. In each pair of collinear bonds on such an atom, one is fully covalent and the other is weaker, but still directional. The two bonds are intrinsically related because they exchange electron density, similarly to the donor–acceptor interactions. During defect transport, the stronger and weaker bond exchange identities, resulting in bond switching not unlike the Grotthuss mechanism of bond switching in water. The electronic states residing on these mobile coordination defects are thus an intrinsic feature of transport in $pp\sigma$-bonded melts and glasses. In contrast, bond switching in known tetrahedrally bonded semiconductors does not occur because the bonds in these materials are homogeneously saturated throughout, excluding the possibility of intrinsic states in these materials, consistent with our earlier conclusions.[9] Note that all types of glassformers host the high-strain interfacial regions that separate low free energy aperiodic configurations and are intrinsic to activated transport. Yet glassformers exhibiting distorted octahedral coordination appear to be unique in their ability to host topological electronic states. The corresponding glasses are thus expected to exhibit anomalies that we have associated with these electronic states,[9] including light-induced electron spin resonance. This expectation is consistent with the variation of the magnitude of light-induced anomalies across the Ge_xSe_{1-x} series[42] for $1/3 < x < 1/2$, which display coordination ranging from tetrahedral (smaller x) to distorted octahedral (larger x). In this series, the octahedral ordering seems to correlate with the light-induced *ESR* and vice versa for the tetrahedral bonding.[43]

The coordination defects exhibit topological features, such as stability against annihilation, if there is a misalignment in the motion of two defects. This peculiarity is related to another topological feature of these states, which is especially transparent in the continuum limit of Eq. (6):[9] $\mathcal{H} = -iv\sigma_3\partial_x + \Delta(x)\sigma_1 + \epsilon(x)\sigma_2$. Here, σ_i are the Pauli matrices, while $-iv\sigma_3\partial_x$, $\Delta(x)$, and $\epsilon(x)$ correspond, respectively, to the kinetic energy, local one-particle gap and variation in electronegativity. The local gap $\Delta(x)$ is space dependent and, in fact, switches sign at the defect, thus corresponding to a rotation of a vector (Δ, ϵ). The orientation angle of this vector is the topological phase associated with the defect. The phases of defects traveling along different paths can not cancel, resulting in a stability against annihilation.

Finally, what are the implications of the present results for direct molecular modeling of amorphous chalcogenides and pnictides? Parent structures differing only by defect locations can be used as the initial configurations for *MD* simulations and may, conceivably, help find transition state configurations corresponding to realistic quenching rates. Yet even assuming the interactions can be estimated accurately and efficiently, the problem is still very computationally expensive, as highlighted by the present work: the number of defectless parent structures, although sub-thermodynamic, is still very very large. We have seen it is plausible that these structures comprise the elusive Kauzmann state for these systems.

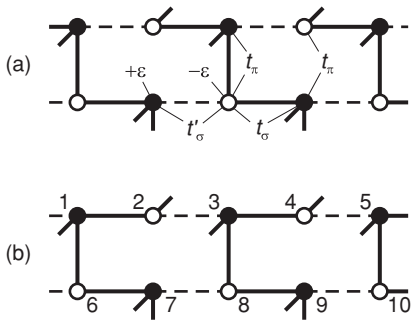

FIG. 13. Double chain interacting via $pp\pi$-overlaps: the configuration (a) is lower in energy than (b) due to $pp\pi$-interaction.

APPENDIX A: THE $pp\pi$-INTERACTION

When the coordination is exactly octahedral, Π-shaped bonds patterns, such as those formed by atoms 2-1-6-7 and 4-3-8-9 in Fig. 13(b), give rise to an additional energy cost stemming from the $pp\pi$-interaction, as explained in the following. It is partially owing to this cost, for instance, that the layers of $AsSe_3$ pyramids in the actual structure of As_2Se_3 are so greatly puckered, see Figs. 7–9 of Ref. 1. To elucidate the origin and estimate the strength of the $pp\pi$-interaction, we consider for concreteness the configurations shown in Fig. 13, periodically continued along the double chain. Only atomic p-orbitals lying in the plane of the figure are considered; these orbitals host two electrons per atom. The nonzero entries of the Hamiltonian matrix are indicated in Fig. 13(a); the notations are from Ref. 1. The total energy of the configuration in Fig. 13(a) can be expanded in a series in terms of the ratios t'_σ/t_σ and t_π/t_σ. In the second order in the expansion, the total energy is the sum of three contributions (assuming $\epsilon = 0$): The covalent bond energy is $-2t_\sigma$ per bond, the secondary bond energy equals $-(t'_\sigma)^2/2t_\sigma$ per bond, and the contribution due to the $pp\pi$-interaction is given by

$$-\frac{t_\pi^2}{2t_\sigma} \tag{A1}$$

per each vertical pair of atoms. One can similarly show that the energy of the configuration in Fig. 13(b) has the same contributions as in (a) except the stabilizing contribution from Eq. (A1), owing to the Π-shaped motifs. As a result, the configuration in Fig. 13(b) is less energetically favorable. According to Eq. (A1), such a Π motif generically costs about 0.1 eV; typical values of the transfer integrals can be found, e.g., in Table I of Ref. 1. This fact can be interpreted equally well either as stabilization due to the staircase motifs in configuration (a) or destabilization due to the Π motifs in configuration (b).

The presence of the $pp\pi$-interaction generally affects the energetics of defect movement, as could be seen in Fig. 13. The top chains in panels (a) and (b) can be obtained from each other by switching all the bonds, as could be achieved, for instance, by moving a malcoordination defect along the chain. As a consequence, the motion of such a defect is subject to

a uniform potential. Now, each structural transition in a supercooled melt is accompanied by the creation of two defects of opposite charge and malcoordination.[9] It follows from the above discussion that in the worst case scenario, the cost of separating two defects scales linearly with the distance, i.e., as $N^{1/3}$, where N is the size of the rearranged region. The scaling of this cost is clearly subdominant to that of the mismatch penalty term $\gamma N^{1/2}$ from Eq. (1). Furthermore, at large enough N, it will be energetically preferable to remove the Π patterns separating the original pair of defects by inserting another pair of malcoordination defects between them. By this mechanism, which is not unlike the mechanism of quark confinement, the cost of the Π patterns is limited by a fixed number which is comparable, but smaller than the typical energy of the interface, i.e., $\gamma N^{1/2}$. We suggest the actual effect of the Π-configurations is yet smaller. Indeed, distinct liquid configurations should have, on the average, the same number of Π-configurations, implying the defect movements are subject to a zero bias, on average. As a result, the magnitude of the overall bias for defect separation scales at most with a square root of the distance, leading to a correction to the energy cost of the reconfiguration that is proportional to $(N^{1/3})^{1/2} = N^{1/6}$. This correction is clearly inferior to the $\gamma N^{1/2}$ term.

ACKNOWLEDGMENTS

The authors thank David M. Hoffman, Thomas A. Albright, Peter G. Wolynes, and the anonymous Reviewer for helpful suggestions. We gratefully acknowledge the Arnold and Mabel Beckman Foundation Beckman Young Investigator Award, the Donors of the American Chemical Society Petroleum Research Fund, and NSF Grant CHE-0956127 for partial support of this research.

[1] A. Zhugayevych and V. Lubchenko, J. Chem. Phys. **133**, 234503 (2010).
[2] K. Shimakawa, A. Kolobov, and S. R. Elliott, Adv. Phys. **44**, 475 (1995).
[3] M. Wuttig and N. Yamada, Nature Mater **6**, 824 (2007).
[4] D. M. Salinga, B. Grabowski, T. Hickel, J. Neugebauer, and M. Wuttig, Nature Mater **7**, 972 (2008).
[5] V. Lubchenko and P. G. Wolynes, Annu. Rev. Phys. Chem. **58**, 235 (2007).
[6] L. Berthier, G. Biroli, J.-P. Bouchaud, L. Cipelletti, D. El Masri, D. L'Hôte, F. Ladieu, and M. Perino, Science **310**, 1797 (2005).
[7] C. Dalle-Ferrier, C. Thibierge, C. Alba-Simonesco, L. Berthier, G. Biroli, J.-P. Bouchaud, F. Ladieu, D. L'Hôte, and M. Perino, Phys. Rev. E **76**, 041510 (2007).
[8] S. Capaccioli, G. Ruocco, and F. Zamponi, J. Phys. Chem. B **112**, 10652 (2008).
[9] A. Zhugayevych and V. Lubchenko, J. Chem. Phys. **132**, 044508 (2010).
[10] V. Lubchenko and P. G. Wolynes, Adv. Chem. Phys. **136**, 95 (2007).
[11] R. Evans, Adv. Phys. **28**, 143 (1979).
[12] Y. Singh, J. P. Stoessel, and P. G. Wolynes, Phys. Rev. Lett. **54**, 1059 (1985).
[13] V. Lubchenko and P. G. Wolynes, J. Chem. Phys. **119**, 9088 (2003).
[14] X. Xia and P. G. Wolynes, Proc. Natl. Acad. Sci. U.S.A. **97**, 2990 (2000).
[15] F. A. Lindemann, Phys. Z. **11**, 609 (1910).
[16] C. A. Angell, K. L. Ngai, G. B. McKenna, P. F. Millan, and S. W. Martin, Appl. Phys. **88**, 3113 (2000).
[17] C. A. Angell, J. Phys.: Condens. Matter **12**, 6463 (2000).
[18] T. R. Kirkpatrick, D. Thirumalai, and P. G. Wolynes, Phys. Rev. A **40**, 1045 (1989).
[19] V. Lubchenko and P. G. Wolynes, J. Chem. Phys. **121**, 2852 (2004).
[20] V. Lubchenko and P. G. Wolynes, Phys. Rev. Lett. **87**, 195901 (2001), cond-mat/0105307.
[21] V. Lubchenko, J. Phys. Chem. B **110**, 18779 (2006).
[22] M. Tatsumisago, B. L. Halfpap, J. L. Green, S. M. Lindsay, and C. A. Angell, Phys. Rev. Lett. **64**, 1549 (1990).
[23] R. Richert and C. A. Angell, J. Chem. Phys. **108**, 9016 (1998).
[24] T. R. Kirkpatrick and P. G. Wolynes, Phys. Rev. B **36**, 8552 (1987).
[25] J. Stevenson and P. G. Wolynes, arXiv:1006.5840v1.
[26] U. Tracht, M. Wilhelm, A. Heuer, H. Feng, K. Schmidt-Rohr, and H. W. Spiess, Phys. Rev. Lett. **81**, 2727 (1998).
[27] E. V. Russel and N. E. Israeloff, Nature (London) **408**, 695 (2000).
[28] M. T. Cicerone and M. D. Ediger, J. Chem. Phys. **104**, 7210 (1996).
[29] S. Ashtekar, G. Scott, J. Lyding, and M. Gruebele, J. Phys. Chem. Lett. **1**, 1941 (2010).
[30] J. K. Burdett and T. J. McLarnan, J. Chem. Phys. **75**, 5764 (1981).
[31] J. K. Burdett, *Chemical Bonding in Solids* (Oxford University Press, New York, 1995).
[32] J. K. Burdett and S. Lee, J. Am. Chem. Soc. **105**, 1079 (1983).
[33] W. Kauzmann, Chem. Rev. **43**, 219 (1948).
[34] R. J. Baxter, *Exactly Solved Models in Statistical Mechanics* (Academic Press, London, 1982).
[35] V. Lubchenko and P. G. Wolynes, "Comment on the "novel isotope effects observed in polarization echo experiments in glasses," (2004), cond-mat/0407581.
[36] MOPAC2009, J. J. P. Stewart, *Stewart Computational Chemistry*, Colorado Springs, CO, USA, http://OpenMOPAC.net (2008).
[37] H. Takayama, Y. R. Lin-Liu, and K. Maki, Phys. Rev. B **21**, 2388 (1980).
[38] J. Stevenson and P. G. Wolynes, J. Phys. Chem. B **109**, 15093 (2005).
[39] D. Bevzenko and V. Lubchenko, J. Phys. Chem. B **113**, 16337 (2009).
[40] M. Kastner, D. Adler, and H. Fritzsche, Phys. Rev. Lett. **37**, 1504 (1976).
[41] R. A. Street and N. F. Mott, Phys. Rev. Lett. **35**, 1293 (1975).
[42] Y. Shimoi and H. Fukutome, J. Phys. Soc. Jpn. **59**, 2790 (1990).
[43] S. I. Simdyankin, S. R. Elliott, Z. Hajnal, T. A. Niehaus, and T. Frauenheim, Phys. Rev. B **69**, 144202 (2004).
[44] A. J. Heeger, S. Kivelson, J. R. Schrieffer, and W. P. Su, Rev. Mod. Phys. **60**, 781 (1988).
[45] P. S. Salmon, J. Non-Cryst. Solids **353**, 2959 (2007).
[46] F. Mollot, J. Cernogora, and C. Benoit à la Guillaume, Philos. Mag. B **42**, 643 (1980).
[47] See supplementary material at http://dx.doi.org/10.1063/1.3511708 for an illustration of the HOMO and LUMO, the spatial variation of the electrostatic potential in a double chain of passivated arsenics, and comparison between the results of geometry optimization for several chain lengths of the $(AsH_2)_n$ chain.

Supplementary Material for
Molecular basis of the glass transition in pnictide and chalcogenide semiconductor alloys. Part II: The intrinsic electronic midgap states.

by Andriy Zhugayevych and Vassiliy Lubchenko
Chemistry Department, University of Houston, TX 77204-5003
(Dated: October 12, 2010)

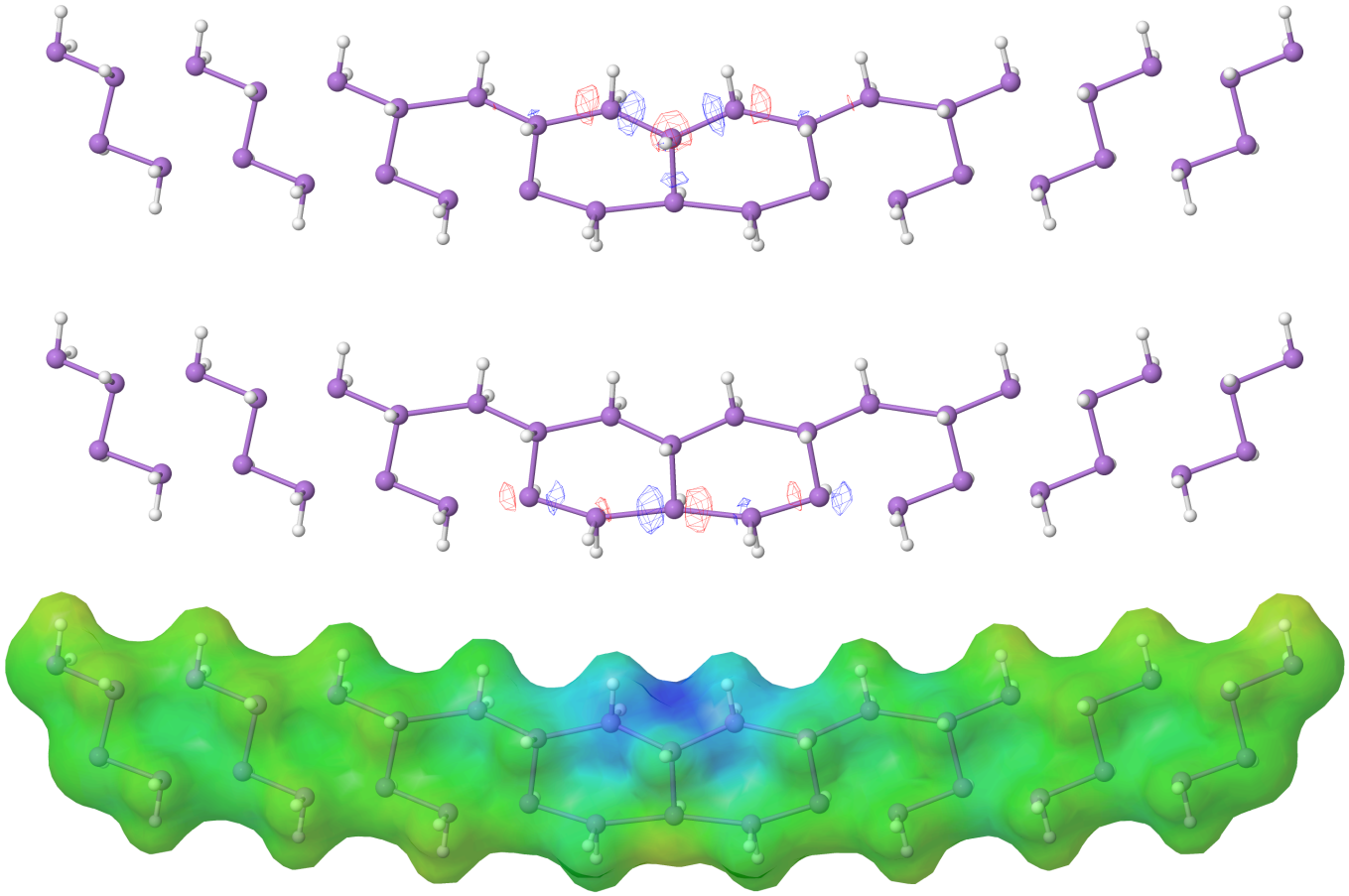

FIG. 1: Local charge distribution at a topologically stable pair of an over- and under-coordinated arsenic in a double chain of hydrogen-passivated arsenics from Fig. 10 of the main text. The LUMO and HOMO are shown in the top and middle panels respectively. The electrostatic potential is shown in the bottom panel, red and blue colors corresponding to positive and negative values respectively.

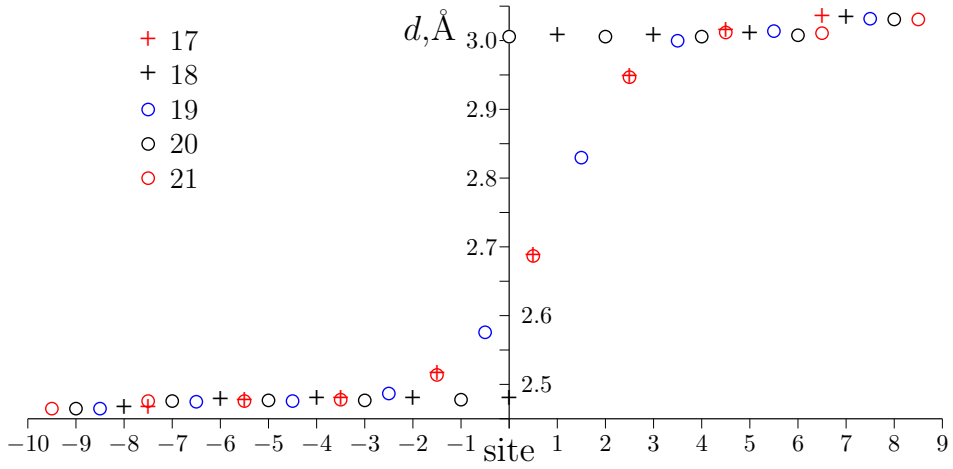

FIG. 2: Site dependence of As-As bond lengths in a $(AsH_2)_n$ chain for several chain lengths is shown, to partially assess the sensitivity of the calculation to the chain length, n. (See the main text for calculational details.) For the reader's reference we note that the energy gradients in the geometry-optimized chains were about 0.01 kcal/mol/Å for even n, and 0.001 kcal/mol/Å for odd n.